Journal of Nuclear Materials 390–391 (2009) 516–519

Contents lists available at ScienceDirect

Journal of Nuclear Materials

journal homepage: www.elsevier.com/locate/jnucmat

On the secular density rises in NBI-heated H-mode plasmas in NSTX

V.A. Soukhanovskii [a,b,*], R.E. Bell [b], C. Bush [c], R. Kaita [b], H.W. Kugel [b], B.P. LeBlanc [b], R. Maingi [c], R. Raman [d], A.L. Roquemore [b], NSTX Research Team

[a] Lawrence Livermore National Laboratory, Livermore, CA, USA
[b] Princeton Plasma Physics Laboratory, Princeton, NJ, USA
[c] Oak Ridge National Laboratory, Oak Ridge, TN, USA
[d] University of Washington, Seattle, WA, USA

ARTICLE INFO

PACS:
52.40.Hf
52.55.fa
52.55.dy

ABSTRACT

Plasma–wall interaction analysis is developed at the National Spherical Torus Experiment. At present, poloidally separated recycling and neutral pressure measurements are used to characterize recycling flux trends. The causes of monotonic density increases observed in initial phases of H-mode discharges at $t \leqslant 0.2$–0.6 s appear to be the monotonically increasing source in the divertor, and particle containment time τ_p^* long in comparison with discharge duration. The ratio of the wall flux to divertor flux is low throughout the density increase phase except in the initial segment, when dN_e/dt is highest and magnitudes of the wall and divertor fluxes are similar.

1. Introduction

Core plasma density control in divertor tokamaks is accomplished by changing the relative magnitude of scrape-off layer (SOL) and divertor particle sources and sinks through fueling and pumping [1]. Particle removal is achieved by either active divertor cryopumping, or through passive pumping by the unsaturated wall. To achieve the pumping wall state, various conditioning techniques, such as the helium glow discharge cleaning (GDC) and metal gettering, including lithium coatings, are commonly used [2]. An essential element of the National Spherical Torus eXperiment (NSTX) research program is the development of lithium evaporative coating techniques [3,4] for plasma density control. The density control is desirable for low density n_e and low collisionality H-mode plasma scenarios that will be used to study the physics of non-inductive current drive and confinement and their projections for the next-step spherical tori (ST) [5]. The arsenal of fueling tools on NSTX includes the low and high field side conventional gas injectors [6,7] and the supersonic gas injector [8]. In this article an initial assessment of recycling flux trends in NSTX is presented, to provide a baseline for present and future experiments with lithium coatings [4] and the liquid lithium divertor (LLD) module.

2. Experiment and method

NSTX is a medium-size ($R = 0.85$ m, $a = 0.67$ m) ST with graphite plasma facing components. In a low triangularity lower single null (LSN) plasma configuration (Fig. 1) the SOL is comprised of the divertor SOL (DSOL), where magnetic field lines connect the inner divertor target to the outer divertor target, and the wall SOL (WSOL) comprising the regions located radially outside the DSOL and limited by the center stack or upper divertor. Typical for this configuration are small ELM H-mode discharges with large out-in heat and particle flux asymmetries [9,10], resulting in the high-recycling regime for the outer DSOL, and the detached regime for the inner DSOL [11,12]. The ionization source is assumed to be in the SOL with a substantial parallel ∇T_e. The WSOL is in the sheath-limited regime with little ionization [13].

Plasma transport regimes as well as particle sources and sinks are often estimated using local particle balance. An analysis of the magnitude of plasma–wall contact, or SOL perpendicular ion fluxes, has been developed analytically [14–16], and applied to tokamak experimental data [17–19]. The technique is termed 'window-frame', as it estimates the perpendicular ion wall flux $\Gamma_\perp$ through the 'window pane', based on the continuity equation (particle balance) considerations for an ionization-free SOL and measurements of the parallel flux to the 'window-pane'. However, a number of ST SOL geometry features makes the application of this technique impossible in NSTX. The DSOL is always in direct contact with the inner wall, and the quasi-continuous poloidal extent of WSOL makes it difficult to separate the inner and outer WSOL fluxes.

* Corresponding author. Address: Princeton Plasma Physics Laboratory, MS34, P. O. Box 451, Princeton, NJ 08543, USA.
E-mail address: vlad@llnl.gov (V.A. Soukhanovskii).

0022-3115/$ - see front matter © 2009 Elsevier B.V. All rights reserved.
doi:10.1016/j.jnucmat.2009.01.067

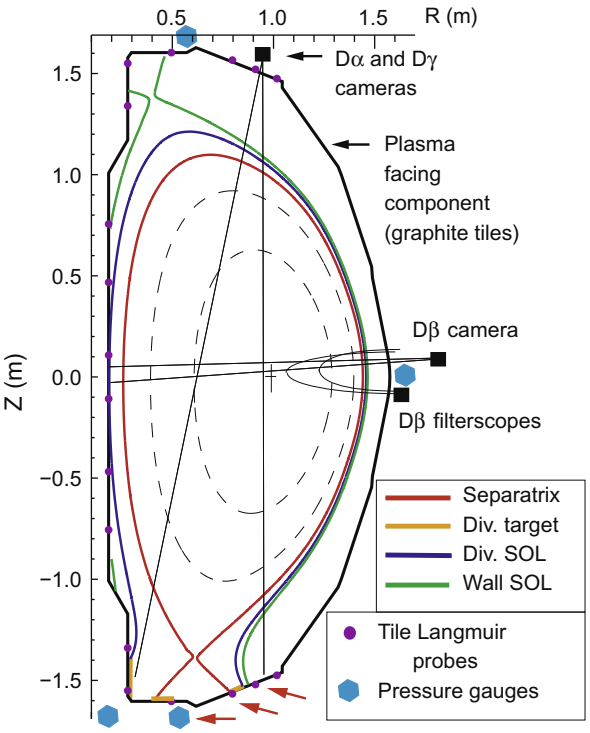

Fig. 1. SOL structure and diagnostics layout.

Lacking high spatial resolution Langmuir probe measurements in the divertor and midplane SOL at present, we retreat to using spectroscopic measurements to estimate recycling fluxes. It is realized that because of poloidal and toroidal non-uniformity of recycling, these measurements would not be as accurate as direct ion flux measurements, however, they should reflect some important functional trends. Ionization fluxes are estimated from the Balmer-α, β emission measurements [11,12,20], averaged over small ELMs, in the divertor and midplane locations (Fig. 1) using the S/XB (ionizations per photon) factors from the ADAS database [21]. This technique assumes that both the electron impact ionization and the excitation of the neutral atom take place in the same volume of ionizing plasma. We use S/XB of 20 for D_α conversions, and S/XB of 100 for D_β conversions. In a similar manner, we use the R/XB factor of 80 recombinations per the Balmer-γ photon [22] to infer the recombination rate in the optically thin detached inner divertor where $T_e = 0.7$–2 eV and $n_e \leqslant 3 \times 10^{20}\,\mathrm{m}^{-3}$ [23].

Consistency check between diagnostic data is an important element of this analysis. Particle flux densities (Γ_i), inferred from D_α, Langmuir probes, and neutral pressure measurements in the outer high-recycling divertor region, are compared in Fig. 3. The parallel ion flux density insident on the Langmuir probe is $\Gamma_{i\parallel} = j^+_{sat}/e = I_{sat}/(e\sin(\alpha)A_{Lp})$, where I_{sat} is the probe ion saturation current, $A_{Lp} = 2.41 \times 10^{-6}\,\mathrm{m}^2$ is the probe tip area, and α is the angle between the magnetic field line and the divertor (probe) surface. Using $\Gamma_{i\parallel}$ and a geometric factor (B_z/B_T), ionization flux is obtained as $\Gamma_i = \Gamma_{i\parallel}(B_z/B_T)$. Neutral pressures are measured in the midplane and divertor by calibrated microion and Penning gauges, respectively [24]. The measurements are not conductance-limited. A standard conversion from pressure P to atomic neutral flux Γ_D is used: $\Gamma_D = (1/4)(P/k_BT)\sqrt{8k_BT/(\pi m)}$, where T is the wall temperature and m is the deutron mass. Errors associated with this estimate technique are discussed in [14]. Returning to Fig. 3, we note that the trends of recycling and ion fluxes are similar. The fluxes, derived from the neutral pressure measured in the private flux region, away from the outer SOL, also follow the same trend. The comparison reveals a systematic discrepancy factor of 1.5–2 between ionization fluxes from Langmuir probe and D_α measurements at the same location. Two factors are likely to contribute to the discrepancy. First, the S/XB factor can vary between 20 and 60 depending on the divertor T_e and n_e. This may lead to an underestimation of the D_α ionization flux in our case. Second, in an ST geometry, both SOL magnetic shear and the associated pitch angle shear are high. At present, the α angles for each probe are derived from the equilibrium reconstruction data using LRDFIT code. An error in the separatrix location is estimated to be about 1 cm. The angle α can change from 20° to 30° over one cm length in the LSN configuration with a low magnetic flux expansion at the outer SP, thus leading to an uncertainty in the derived ion flux. With further development of T_e, n_e analysis of divertor Langmuir probe data, it is expected that the discrepancy factors would be better understood and reduced.

A large difference between the inner and outer midplane fluxes is measured. This is because in the inner WSOL, the measured D_β emission is due to the neutral recycling on the inner wall graphite tiles, while in the outer WSOL, the diffuse midplane emission, not directly associated with a surface source, is measured. Using ionization fluxes inferred from spectroscopy, we construct a continuous poloidal flux density profile, and integrate over the poloidal areas of the outer divertor, inner and outer WSOLs to obtain total particle fluxes.

Core carbon density is measured by the charge exchange recombination spectroscopy system [25]. Deutron density is inferred from the quasi-neutrality condition $Z_{eff} = \sum_i \frac{n_i}{n_e} Z_i^2$ where Z_{eff} due to carbon ($Z = 6$) is assumed.

3. Results and discussion

In NSTX, a monotonic persistent density increase, referred hereforth as the secular density rise, is observed in NBI-heated gas-fueled H-mode discharges [9,10] despite helium GDC wall conditioning between discharges and an apparent pumping state of graphite walls, as inferred from the 0D particle balance analysis [26]. Whereas n_e can be varied within a limited range by changing the HFS gas puffing rate, the dN_e/dt term, where N_e is the total electron inventory, remains high, in the range $(0.2$–$3) \times 10^{21}\,\mathrm{s}^{-1}$ in small-ELM or ELM-free H-mode discharges with $N_e \leqslant (2$–$6) \times 10^{20}$. The secular density rise in a 0.8 MA, 2 MW NBI-heated H-mode discharge with small ELMs is illustrated in Fig. 2. Both the electron and ion densities (and inventories) monotonically rise throughout a discharge. The rates of rise $d\{N,n\}/dt$ typically decrease with density. The contribution from carbon to the total electron inventory $6 \times N_c$ can be up to 30 % during carbon accumulation in the H-mode pedestal region at a later phase of the discharge. Importantly, plasma stored energy W_{MHD} and energy confinement time τ_E remain nearly constant in the H-mode phase.

The recycling fluxes Γ_i and the inner divertor recombination Γ_R fluxes are compared in Fig. 4. In NSTX, the inner divertor detaches at low density, whereas the outer divertor remains in the high-recycling regime and does not detach even at $n_e \sim n_G$, the Greenwald density [11,12]. Several results are apparent from the figure. The relative magnitude of the divertor and wall fluxes are of the same order of magnitude at low N_e. Wall fluxes remain nearly constant throughout the density scan, while the magnitude of the outer divertor flux increases. In the outer DSOL, average $\Gamma_{Recy} \sim \bar{n}^{\alpha}_e$ with $\alpha \simeq 1.5$–1.9, being close to $\alpha \simeq 2$–3 expected from the two point model of the high parallel ∇T_e DSOL regime [27]. At higher densities, the outer divertor flux appears to be the dominant recycling source, exceeding the combined wall flux by up to 80%.

The recombination flux in the inner detached divertor region appears to be relatively high. The Γ_R also increases with density.

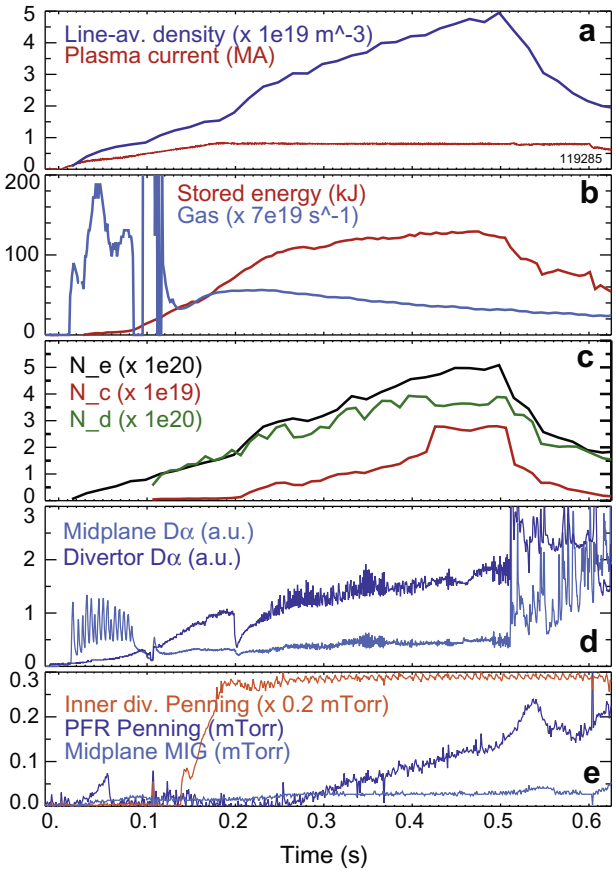

Fig. 2. Time traces of (a) $\bar{n}_e$ and I_p; (b) gas injection rate and W_{MHD}; (c) total electron, deutron and carbon inventories; (d) midplane and divertor D_α signals; (f) neutral pressure signals from inner divertor and private flux region (PFR) Penning gauges and from midplane microion gauge (MIG). Neutral pressure P is converted to deutron flux Γ_D according to $\Gamma_D\ (s^{-1}) = 1.11 \times 10^{25} \times P\ (\text{Torr})$ as described in text.

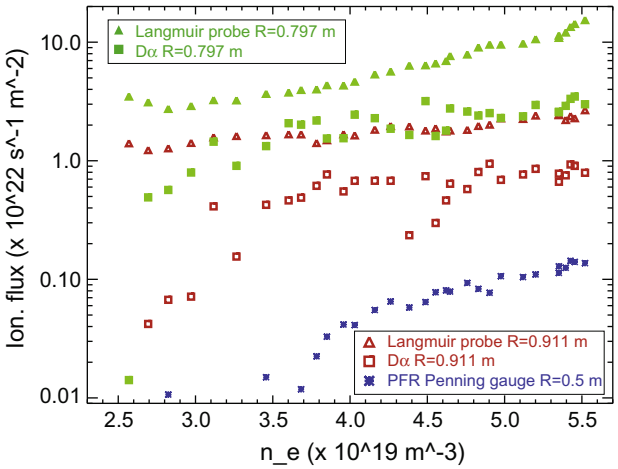

Fig. 3. Ionization flux densities from lower divertor Langmuir probes, D_α, and neutral pressure measurements.

The inner divertor region includes a volume of $\simeq 0.075\,m^3$ of low T_e, high n_e plasma [23]. The high recombination rate of the inner divertor is consistent with high inner divertor neutral pressure (Fig. 2). The inner divertor leg structure is complex: the cold recombining region with high n_e and n_0 is confined between the separatrix, private flux region, and the inner SOL. This strongly-recombining MARFE-like region can act as a limiter [28], with a local ionization front fueling plasma through the X-point region. If a low S/XB ratio of 1–2 is used for the detached divertor D_α intensity, as suggested by experimental studies (e.g., [29,30]), we obtain a large ionization flux $1-1.5 \times 10^{22}\ s^{-1}$. Molecular fluxes in the inner divertor region can also contribute significantly to both ionization and recombination [31]. Thus, we conjecture that the detached inner divertor region can strongly contribute as a fueling source, however, the extent of this contribution is presently unclear.

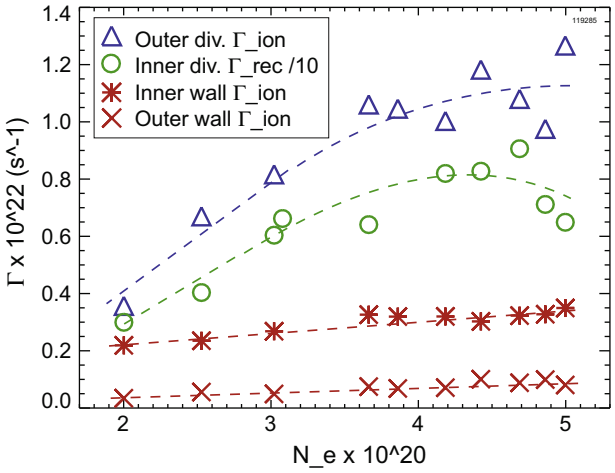

Fig. 4. Integrated ionization and recombination fluxes. Lines are drawn to guide the eye.

The relative fraction of WSOL and DSOL fluxes remains constant ~ 0.3 over a range of density increase rates as shown in Fig. 5, except at the highest dn_e/dt. The highest density rise rate corresponds to the low n_e low recycling phase following the L–H transition at 0.2 s (Fig. 2) when small ELMs are either absent or just forming. During this period, WSOL and DSOL ionization fluxes and the inner divertor recombination flux are of the same order.

To discuss the secular density rises in NSTX, we employ a simple particle balance equation:

$$N_e = \tau_p(S_R + S_g - dN_i/dt) + \tau_p^{NB}(S_{NB} - dN_i^{NB}/dt), \quad (1)$$

where $S_{NB,g,R}$ are ionization sources due to NBI fueling, gas fueling, and recycling. Particle losses are expressed using N_e/τ_p, where the particle confinement time τ_p is different for gas-puffing/recycling

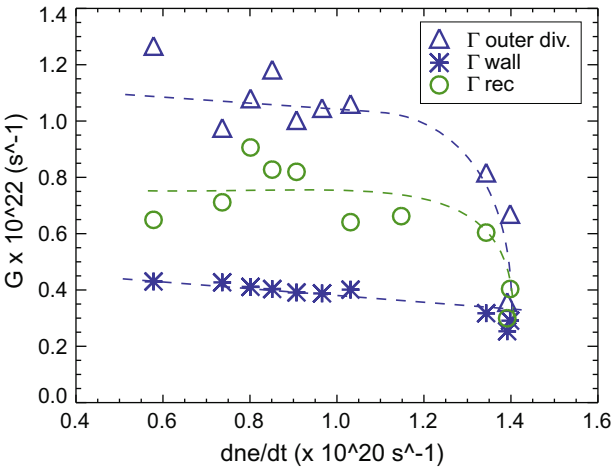

Fig. 5. Total divertor and wall fluxes as function of density rise rate. Lines are drawn to guide the eye.

and fast NBI neutrals. The observed secular density rise in NSTX can be attributed to the increase in the divertor recycling source S_r and to a relatively small loss term N_e/τ_p. Other particle sources are much smaller in magnitude and cannot explain the particle inventory increase [26]. The HFS gas injector rate is $\Gamma_g \leqslant 10^{21}\,s^{-1}$. When multiplied by the fueling efficiency of 0.05–0.15, the resulting ion source S_g is less than the wall source, and significantly less than the divertor source. The NBI contribution is also small: $1.1 \times 10^{20}\,s^{-1}$ per 1 MW of 80 kV NBI (here, the fueling efficiency of nearly 100% was assumed).

If the equation is re-cast using the particle containment time $\tau_p^* = \tau_p/(1-R)$ as

$$\frac{dN_e}{dt} = S - \frac{N_e}{\tau_p^*} \tag{2}$$

an analytic solution would reveal a $N_e(t)$ dependence on τ_p^* magnitude (e.g., [32]). Here we assume that in the high-recycling divertor, the recycling coefficient R is near unity and remains constant. In the case of $t \ll \tau_p^*$, N_e will increase monotonically with time. When $t \gg \tau_p^*$, $N \sim S\tau_p^*$. Order of magnitude estimates with measured N_e and S result in τ_p^* values of hundreds of milliseconds, suggesting that the secular density rise over a short time period $t \leqslant \tau_p^*$ may be affected in part by the large τ_p^* effect [32]. Nonetheless, the secular density rise is observed in most ohmic, L-mode and small ELM or ELM-free H-mode discharges with duration up to 1–1.2 s, regardless of the fueling scheme. Graphite plasma facing component conditioning with ohmic helium discharges appear to have an arresting effect on the secular density rises [33], suggesting that density control could be improved by an optimized between-discharge He GDC.

To summarize, initial results from multiple diagnostics appear to indicate a fairly low ratio between the wall and divertor fluxes in NSTX. The ratio remains nearly constant over a wide density range, except at lower densities when the role of the wall flux appear to be stronger. It is consistent with the analytic plasma–wall interaction model [15] describing the divertor-target recycling as a controlling factor in plasma fueling. The divertor recycling source appears to dominate ion particle balance resulting in the secular density rises. Present results suggest that pumping projections for the liquid lithium divertor module should be carefully examined since at low n_e wall and divertor fluxes appear to be nearly equal. Further analysis, including midplane and divertor Langmuir probe measurements [13], and the two-dimensional SOL transport modeling [34] should provide a firmer basis for the particle flux assessment in NSTX.

Acknowledgements

We thank the entire NSTX Team for plasma, NBI, diagnostic, and engineering operations and support. This research was supported in part by the US Department of Energy under contracts No. DE-AC52-07NA27344, DE-AC02-76CH03073, DE-AC05-00OR22725, and W-7405-ENG-36.

References

[1] ITER Physics Expert Group on divertor, ITER Physics Expert Group on Divertor Modelling and Database, ITER Physics Basis (Eds.), Nucl. Fus. 39 (12) (1999) 2391.
[2] J. Winter, Plasma Phys. Control. Fus. 38 (1996) 1503.
[3] H.W. Kugel, M.G. Bell, J.-W. Ahn, J.P. Allain, R. Bell, J. Boedo, C. Bush, D. Gates, T. Gray, S. Kaye, R. Kaita, B. LeBlanc, R. Maingi, R. Majeski, D. Mansfield, J. Menard, D. Mueller, M. Ono, S. Paul, R. Raman, A.L. Roquemore, P.W. Ross, S. Sabbagh, H. Schneider, C.H. Skinner, V. Soukhanovskii, T. Stevenson, J. Timberlake, W.R. Wampler, L. Zakharov, Phys. Plasmas 15 (5) (2008) 056118.
[4] H.W. Kugel, M.G. Bell, J.-W. Ahn, J.P. Allain, R. Bell, J. Boedo, C. Bush, Paper P2-58, in: Proc. of the 18th PSI Conf., 2008.
[5] J. Menard, M. Bell, R. Bell, S. Bernabei, J. Bialek, T. Biewer, W. Blanchard, J. Boedo, C. Bush, M. Carter, W. Choe, N. Crocker, D. Darrow, W. Davis, L. Delgado-Aparicio, S. Diem, C. Domier, D. D'Ippolito, J. Ferron, A. Field, J. Foley, E. Fredrickson, D. Gates, T. Gibney, R. Harvey, R. Hatcher, W. Heidbrink, K. Hill, J. Hosea, T. Jarboe, D. Johnson, R. Kaita, S. Kaye, C. Kessel, S. Kubota, H. Kugel, J. Lawson, B. Leblanc, K. Lee, F. Levinton, N. Luhmann, R. Maingi, R. Majeski, J. Manickam, D. Mansfield, R. Maqueda, R. Marsala, D. Mastrovito, T. Mau, E. Mazzucato, S. Medley, H. Meyer, D. Mikkelsen, D. Mueller, T. Munsat, J. Myra, B. Nelson, C. Neumeyer, N. Nishino, M. Ono, H. Park, W. Park, S. Paul, T. Peebles, M. Peng, C. Phillips, A. Pigarov, R. Pinsker, A. Ram, S. Ramakrishnan, R. Raman, D. Rasmussen, M. Redi, M. Rensink, G. Rewoldt, J. Robinson, P. Roney, A. Roquemore, E. Ruskov, P. Ryan, S. Sabbagh, H. Schneider, C. Skinner, D. Smith, A. Sontag, V. Soukhanovskii, T. Stevenson, D. Stotler, B. Stratton, D. Stutman, D. Swain, E. Synakowski, Y. Takase, G. Taylor, K. Tritz, A. Von Halle, M. Wade, R. White, J. Wilgen, M. Williams, J. Wilson, H. Yuh, L. Zakharov, W. Zhu, S. Zweben, R. Akers, P. Beiersdorfer, R. Betti, T. Bigelow, M. Bitter, P. Bonoli, C. Bourdelle, C. Chang, J. Chrzanowski, L. Dudek, P. Efthimion, M. Finkenthal, E. Fredd, G. Fu, A. Glasser, R. Goldston, N. Greenough, L. Grisham, N. Gorelenkov, L. Guazzotto, R. Hawryluk, J. Hogan, W. Houlberg, D. Humphreys, F. Jaeger, M. Kalish, S. Krasheninnikov, L. Lao, J. Lawrence, J. Leuer, D. Liu, G. Oliaro, D. Pacella, R. Parsells, M. Schaffer, I. Semenov, K. Shaing, M. Shapiro, K. Shinohara, P. Sichta, X. Tang, R. Vero, M. Walker, W. Wampler, Nucl. Fus. 47 (10) (2007) 645.
[6] H.W. Kugel, M. Anderson, G. Barnes, M. Bell, W. Blanchard, L. Dudek, D. Gates, R. Gernhardt, R. Maingi, D. Mueller, T. Provost, R. Raman, V. Soukhanovskii, J. Winston, in: Proc. of the 20th IEEE/NPSS Symposium on Fusion Engineering, IEEE, San Diego, CA, 2003.
[7] R. Maingi, C.S. Chang, S. Ku, T. Biewer, R. Maqueda, Plasma Phys. Control. Fus. 46 (2004) A305.
[8] V. Soukhanovskii, H. Kugel, R. Kaita, R. Majeski, A. Roquemore, Rev. Sci. Instrum. 75 (2004) 4320.
[9] R. Maingi, M. Bell, R. Bell, C. Bush, E. Fredrickson, D. Gates, T. Gray, D. Johnson, R. Kaita, S. Kaye, S. Kubota, H. Kugel, C. Lasnier, B. LeBlanc, R. Maqueda, D. Mastrovito, J. Menard, D. Mueller, M. Ono, F. Paoletti, S. Paul, Y.-K. Peng, A. Roquemore, S. Sabbagh, C. Skinner, V. Soukhanovskii, D. Stutman, D. Swain, E. Synakowski, T. Tan, J. Wilgen, S. Zweben, Nuc. Fus. 43 (9) (2003) 969–974.
[10] R. Maingi, S. Sabbagh, C. Bush, E. Fredrickson, J. Menard, D. Stutman, K. Tritz, M. Bell, R. Bell, J. Boedo, D. Gates, D. Johnson, R. Kaita, S. Kaye, H. Kugel, B. Leblanc, D. Mueller, R. Raman, A. Roquemore, V. Soukhanovskii, T. Stevenson, J. Nucl. Mater. 337–339 (2005) 727.
[11] V. Soukhanovskii, R. Maingi, A. Roquemore, J. Boedo, C. Bush, R. Kaita, H. Kugel, B. LeBlanc, S. Paul, G. Porter, N. Wolf, J. Nucl. Mater. 337–339 (2005) 475.
[12] V. Soukhanovskii, R. Maingi, C. Bush, R. Raman, R. Bell, R. Kaita, H. Kugel, C. Lasnier, B. LeBlanc, J. Menard, S. Paul, A. Roquemore, J. Nucl. Mater. 363–365 (2007) 432.
[13] J.-W. Ahn, J.A. Boedo, R. Maingi, V. Soukhanovskii, J. Nucl. Mater. 390–391 (2009) 421.
[14] B. LaBombard, M.V. Umansky, R.L. Boivin, J.A. Goetz, J. Hughes, Nucl. Fus. 40 (2000) 2041.
[15] P.C. Stangeby, Phys. Plasmas 9 (2002) 3489.
[16] P.C. Stangeby, J. Phys. D: Appl. Phys. 36 (2003) 2784.
[17] B. Lipschultz, D. Whyte, B. LaBombard, Plasma Phys. Control. Fus. 47 (2005) 1559.
[18] D.G. Whyte, B.L. Lipschultz, P.C. Stangeby, J. Boedo, D.L. Rudakov, J.G. Whatkins, W.P. West, Plasma Phys. Control. Fus. 47 (2005) 1579.
[19] A. Leonard, J. Boedo, M. Groth, B. Lipschultz, G. Porter, D. Rudakov, D. Whyte, J. Nucl. Mater. 363–365 (2007) 1066.
[20] V.A. Soukhanovskii, A.L. Roquemore, C.H. Skinner, D. Johnson, R. Maingi, C. Bush, F. Paoletti, S. Sabbagh, Rev. Sci. Instrum. 74 (2003) 2094.
[21] H.P. Summers, The ADAS User Manual, version 2.6 http://adas.phys.strath.ac.uk.
[22] J.L. Terry, B. Lipschultz, X. Bonnin, C. Boswell, S.I. Krasheninnikov, A.Y. Pigarov, B. LaBombard, D.A. Pappas, H.A. Scott, J. Nucl. Mater. 266–269 (1999) 30.
[23] V.A. Soukhanovskii, D. Johnson, R. Kaita, A.L. Roquemore, Rev. Sci. Instrum. 77 (2006) 10F127.
[24] R. Raman, H.W. Kugel, R. Gernhardt, T. Provost, T.R. Jarboe, V. Soukhanovskii, Rev. Sci. Instrum. 75 (10) (2004) 4347.
[25] R.E. Bell, Rev. Sci. Instrum. 77 (2006) 10E902.
[26] V.A. Soukhanovskii, R. Maingi, R. Raman, H.W. Kugel, B.P. LeBlanc, A.L. Roquemore, C.H. Skinner, J. Nucl. Mater. 313 (2003) 573.
[27] P.C. Stangeby, The Plasma Boundary of Magnetic Fusion Devices, IoP, Bristol, 2000.
[28] B. Lipschultz, J.L. Terry, C. Boswell, A. Hubbard, B. LaBombard, D.A. Pappas, Phys. Rev. Lett. 81 (1998) 1007.
[29] M. Stamp, S. Erents, W. Fundamenski, G. Matthews, R. Monk, Phys. Scr. T91 (2001) 13.
[30] A. Loarte, R. Monk, J. Martin-Solis, D. Campbell, A. Chankin, S. Clement, S. Davies, J. Ehrenberg, S. Erents, H. Guo, P. Harbour, L. Horton, L. Ingesson, H. Jackel, J. Lingertat, C. Lowry, C. Maggi, G. Matthews, K. McCormick, D. O'Brien, R. Reichle, G. Saibene, R. Smith, M. Stamp, D. Stork, G. Vlases, Nucl. Fus. 38 (1998) 331.
[31] E. Hollmann, S. Brezinsek, N. Brooks, M. Groth, A. McLean, A. Pigarov, D. Rudakov, Plasma Phys. Control. Fus. 48 (2006) 1165.
[32] R. Maingi, K. Tritz, E. Fredrickson, J. Menard, S. Sabbagh, D. Stutman, M. Bell, R. Bell, C. Bush, D. Gates, D. Johnson, R. Kaita, S. Kaye, H. Kugel, B. LeBlanc, D. Mueller, R. Raman, A. Roquemore, V. Soukhanovskii, Nucl. Fus. 45 (2005) 264.
[33] H. Kugel, M. Bell, R. Bell, C. Bush, D. Gates, T. Gray, R. Kaita, B. Leblanc, R. Maingi, R. Majeski, D. Mansfield, D. Mueller, S. Paul, R. Raman, A. Roquemore, S. Sabbagh, C. Skinner, V. Soukhanovskii, T. Stevenson, L. Zakharov, J. Nucl. Mater. 363–365 (2007) 791.
[34] D.P. Stotler, J.P. Allain, J.N. Brooks, H.W. Kugel, R. Maingi, T.D. Rognlien, V.A. Soukhanovskii, L.E. Zakharov, J. Nucl. Mater. 390–391 (2009) 421.